J Forensic Sci, September 2003, Vol. 48, No. 5
Paper ID JFS2002212_485
Available online at: www.astm.org

CASE REPORT

Graham A. Walsh,[1] *M.S.; Osman T. Inal,*[1] *Ph.D.; and Van D. Romero,*[2] *Ph.D.*

A Potential Metallographic Technique for the Investigation of Pipe Bombings*

ABSTRACT: This study was conducted in an attempt to develop a metallographic method for the investigation of pipe bombings. Three common pipe materials, ASTM A53 steel, AISI 304L stainless steel, and 6061-T6 aluminum, were shock-loaded using five high explosives and three propellants. The explosives used were ANFO, Composition C4, C6 detasheet, nitroglycerine-based dynamite, and flake TNT. The propellants used were FFFFg black powder, Red Dot smokeless powder, and Turbo Fuel A.

The post-blast microstructure, hardness, and, in the case of 304L, transformed martensite content were examined for each test. The damage done to the microstructure was found to increase with increasing detonation velocity of the explosives and increase in pressure generated by the shock-metal interaction. Material hardness and, in the case of 304L, martensite content showed a sharp increase followed by a plateau as the shock pressure and detonation velocity increased.

KEYWORDS: forensic science, materials science, metallurgy, metal-shock interactions, pipe bombs, improvised explosive devices, explosives, black powder, smokeless powder

In post-blast investigations, fragments from the explosive device itself are valuable sources of information and are therefore closely examined. Studies have been conducted tying the size distribution and blast pattern of pipe bomb fragments to the type of explosive fill used (1). The examination of chemical residues from fragments is also a well-studied, well-documented technique that has often been used to identify the type of explosive used in criminal bombings (2–5). The fragments themselves hold valuable, metallurgical evidence as well, in the form of the post-blast microstructure and hardness, which may be used to characterize explosive fills.

The microstructural response of metals to shock has been widely studied in the past, in applications such as explosive welding (6–8), shock hardening (9–11), and in the formation of explosively formed projectiles and shaped charges (12–15). The conditions the metals are subjected to in these fields is quite different than those seen in a bombing. The materials used in the aforementioned studies are generally very high purity metals, machined to meet strict tolerances and designed to avoid complex shock interactions by, in the case of shock hardening, surrounding the specimen with large momentum traps. In a bombing, the materials are generally inexpensive pipes purchased at a hardware store, and there are no carefully machined momentum traps. Despite these differences, some of the findings from explosive metalworking were found to be quite useful in this study.

It has been shown that the grain structures of materials subjected to an explosive shock are altered by the shock, showing high amounts of deformation and material flow. In some cases the deformation in the metal is high enough that, coupled with a high degree of shock heating, recrystallization has been observed (12,13). Another common material response to explosive shock is deformation twinning. This has been seen in explosive welding (6) and in the study of explosively formed projectiles (14). Adiabatic shear bands are regions of highly concentrated plastic deformation within a material and are often formed in both ferritic and austenitic steels when subjected to dynamic deformation (16,17). In 304L stainless steel, one of the materials used in this study, there is a shock-induced phase transformation from γ austenite to α' martensite that may be observed and quantified by the use of X-ray diffraction (9,18,19). When a material is shocked, many defects are created, hardening the material (9,20,21). In materials with low stacking fault energy, many partial dislocations are formed when the material is shocked, which inhibits the movement of dislocations in the material, resulting in dislocation entanglements and a high degree of shock-hardening (22,23). All of these observed phenomena (degree of deformation, twin density, shear band density, the amount of post-blast martensite, dislocation density, and residual hardness) increase with both shock pressure and pulse duration (6–23).

In this study, eight fillers, consisting of five high explosives and three propellants, were tested in pipes composed of ASTM A53 galvanized steel, AISI 304L stainless steel, and 6061-T6 aluminum. The fragments from these tests were collected in soft catch packets, which consisted of twenty-four 33 by 66-cm rectangles of

[1] Department of Materials and Metallurgical Engineering, New Mexico Institute of Mining and Technology, Socorro, NM.
[2] Department of Physics, New Mexico Institute of Mining and Technology, Socorro, NM.

* Supported by the U.S. Department of Justice, Office of Justice Programs, through Contract Number 98-TG-CX-0001.

Received 21 June 2002; and in revised form 31 Jan. 2002 and 15 March 2003; accepted 15 March 2003; published 4 Aug. 2003.

Celotex® bound together to form a 33-cm-thick packet. The resulting microstructures and hardnesses of the fragments were examined. This was done in an effort to correlate an explosive property, such as the detonation velocity, to a material response. If one were able to make such a correlation, it would be possible to use these metallurgical methods to give a range of possible detonation velocities of the explosive fill. This would be valuable information if used for screening for such chemical methods as high-pressure liquid chromatography (HPLC).

Methods

Materials Selection

The metal pipes selected for this study were purchased at hardware and plumbing supply stores as pre-threaded nipples with end caps. The metals selected were ASTM A53 galvanized steel, 6061-T6 aluminum,and AISI 304L stainless steel.

The explosives selected were ANFO, Composition C4, dynamite, detasheet, and TNT. The propellants consisted of black powder, smokeless powder, and Turbo Fuel A.

Experimental Setup

For the five high explosives and the two powders, 10.2-cm (4-in.)-long, 5.1-cm (2-in.) inner diameter schedule 40 nipples were filled with explosives, capped and initiated with nonel detonators (in the case of the high explosives) or squibs (in the case of the powders). Four replicas were done for each metal/explosive combination and four fragments randomly selected (out of the soft catch packets) from each test for analysis. Four soft catch packets were placed around each pipe at a distance of approximately 1 m.

The test setup for the Turbo Fuel A tests was much more complicated. The pipe was 122 cm long and the wall machined down to 0.13 cm. The end caps were secured to the pipe using JB Weld®, and a feedhole was drilled and tapped in each cap. A Swagelok® fitting was inserted into each cap and secured using Teflon® tape. After inserting 30 mL of Turbo Fuel A into the pipe, a stainless steel gas feed line was inserted into one fitting and two electric matches into the other. The entire apparatus was wrapped in heat tape and insulation and heated to 204°C (400°F) and allowed to stay at temperature for 20 min. After 20 min, the pipe was filled with O_2 gas to a pressure of 4.8 MPa (700 psi) and the matches ignited. This test was only performed using the A53 pipe.

Sample Preparation

After the fragments were collected, specimens were set in 3.81-cm-diameter Lucite® mounts, two per mount, to examine the cross section and the face that was subjected to the explosion. Reference samples, which did not see any shock, were also mounted and treated in the same fashion. The samples were ground down to 1200 grit using SiC paper and then polished down to 0.3 μm using an alumina slurry. The samples were then etched using Nital for the A53 steel, Vilella's reagent for the 304L, and Keller's reagent for the aluminum; the compositions of these etchants can be found in Tables 1, 2, and 3, respectively (24).

Sample Analysis

Optical micrographs were taken at magnifications ranging from X50 to X400. The mounted specimens were then placed into a Leco M400 microhardness tester fitted with the Knoop indentor, using a load of 10 g and a dwell time of 10 s and the hardness measured at many points along the cross section to give a hardness profile. Unmounted samples from the galvanized and stainless steel tests were tested using a Macromet Rockwell macrohardness tester using the B (for the galvanized steel) and C (for the stainless steel) scales. Samples from the 304L tests were also examined using a Siemens Kristalloflex 810 X-ray diffractometer through a 2Θ range of 40 to 95° using Cu K_α radiation, a step size of 0.05° and a dwell time of 1 s. Quantitative analysis was performed using the direct comparison method (25) to determine the amount of shock induced α′ martensite generated by the passage of the shock wave.

TABLE 1—*The composition of Nital, the etchant used for A53 steel.*

Constituent	Ethanol	Nitric Acid	DI Water
Volume %	87	5.9	7.1

TABLE 2—*The composition of Vilella's reagent, used to etch 304L.*

Constituent	Glycerol	Nitric Acid	HCl	DI Water
Volume %	43.5	10.8	10.7	35

TABLE 3—*The composition of Keller's reagent, used to etch 6061 aluminum.*

Constituent	DI Water	Nitric Acid	HCl	HF
Volume %	67.1	20	9.8	3.1

TABLE 4—*The density, shock Hugoniot parameters and SFE of each metal studied.*

Metal	ρ_0 (g/cm^3)	C_0 (km/s)	S	SFE (mJ/m^2)
A53 steel	7.850	3.574	1.92	50–70
304L stainless	7.903	4.57	1.49	15–30
6061-T6 Al	2.703	5.35	1.34	~200

Results and Discussion

Shock Parameters

The three main shock properties of interest in this study were the detonation velocity of the explosives, the generated pressure, and shock heating, which are functions of the metal/explosive combinations being studied.

Shock parameters and some other properties of the metals studied, including stacking fault energy (SFE), are listed in Table 4. The bulk sound speed (C_0) and empirical constant (s) dictate the response of a material's particle velocity (u) and specific volume (V), which is the inverse of the density, to a shock by the following equations (7,25):

$$P = \rho_0 C_0 (u - u_0) + \rho_0 s (u - u_0)^2$$

$$P = C_0^2 (V_0 - V)\{V_0 - s(V_0 - V)\}^{-2}$$

where u_0 is the initial particle velocity (in this case it is zero), and V_0 is the initial specific volume, which is equal to the inverse of the material density.

The pressure-particle velocity plots and pressure-specific volume plots (called Hugoniots), which result from the above calculations, are shown in Figs. 1 and 2 for each of the metals. The post-mortem heat generated in a material can be calculated from the pressure-specific volume Hugoniot as shown in Fig. 2. When a material is shocked, it does not follow the smooth path of the Hugoniot up to pressure; rather, it jumps along what is called the Rayleigh line. However, the material unloads back to essentially zero pressure and a value very close to the initial volume along the smooth curve of the Hugoniot. The area under the Hugoniot bounded by the beginning and ending pressures is the work re-

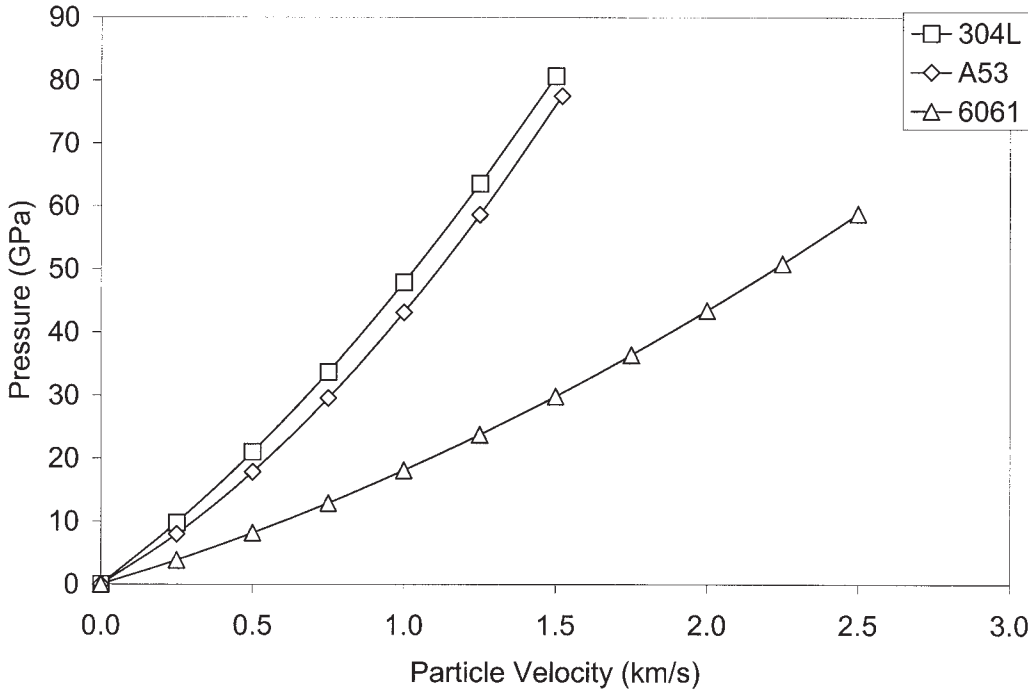

FIG. 1—*The pressure-particle velocity Hugoniots for A53 galvanized steel, 304L stainless steel, and 6061-T6 aluminum.*

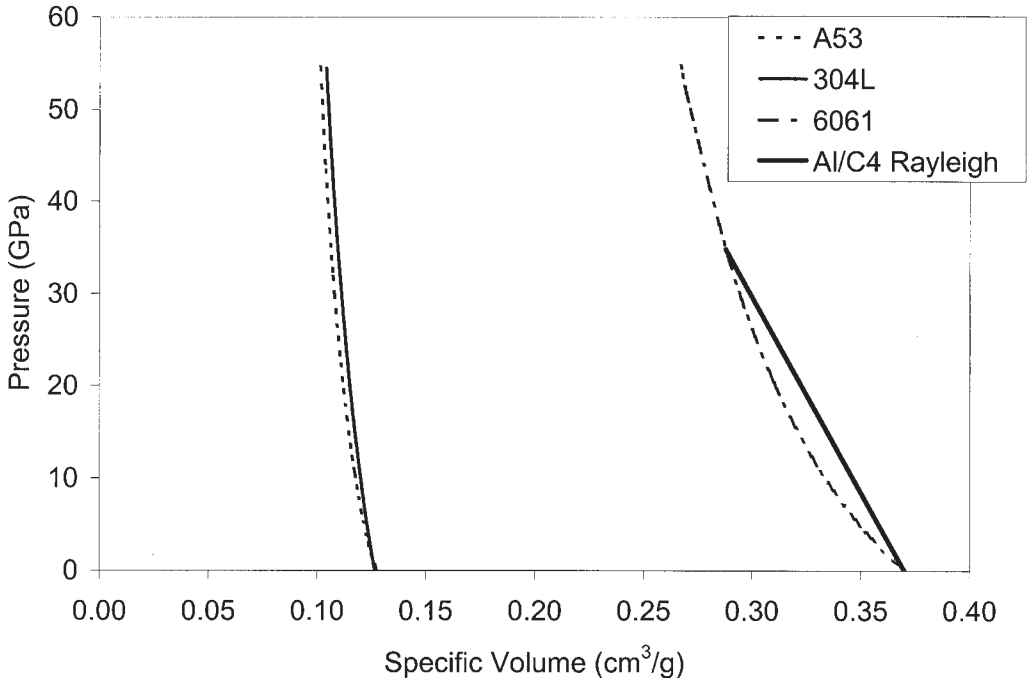

FIG. 2—*The pressure-specific volume Hugoniots for A53 galvanized steel, 304L stainless steel, and 6061-T6 aluminum. The Rayleigh line shown is for the aluminum/composition C4 combination.*

quired to deform the material, while the area between the Hugoniot and the Rayleigh line is excess work that is wasted as heat. The concavity of the pressure-specific volume Hugoniot, therefore, dictates the amount of shock heating seen by a material (7,25). A sample Rayleigh line for the aluminum/composition C4 interaction is shown along with the pressure-specific volume plots in Fig. 2.

A comparison of explosive properties is shown in Table 5. From the values listed in Table 2, the reacted pressure-particle velocity Hugoniots for each of the high explosives can be calculated using the equation:

$$P = (2.412\ P_{CJ}) - \left(\frac{1.7315\ P_{CJ}}{u_{CJ}}\right)u + \left(\frac{0.3195\ P_{CJ}}{u_{CJ}^2}\right)u^2$$

where $u_{CJ} = \dfrac{P_{CJ}}{\rho_o V_D}$

and used along with the pressure-particle velocity Hugoniots of the metals to determine numerically the pressure generated in each material due to the shock generated by the high explosives (7,25). This can also be determined graphically, as shown in Fig. 3, by plotting the pressure-particle velocity Hugoniots for all the explosives and metals and reading the pressures where any two of the lines intersect.

TABLE 5—*The density, detonation velocity, CJ pressure, and TNT equivalent for each of the explosives studied in order from most powerful to least powerful.*

Explosive	ρ (g/cm^3)	Det Vel (km/s)	CJ Pressure (GPa)	TNT Equivalent
Comp. C4	1.60	8.19	28	1.34
Detasheet	1.47	7.00	21	1.01
TNT	1.47	6.48	15	1.00
Dynamite	1.38	5.33	10	0.96
ANFO	0.87	4.79	5.6	0.82

The pressure generated in the metal is used to determine the shocked volume of the sample, which can be used to calculate the temperature change due to shock heating. This relationship is illustrated in Fig. 4, which plots the degree of shock heating produced by shocks of various strengths in each of the metals (26).

Using the relationships described above it is also possible to determine the pressure generated by a metal/metal collision (7,25). These calculations show that the difference in the internal pressure of the metal shocked by an explosive and that of a metal/metal collision differ greatly, which is why samples were collected in soft catch packets. By equating the pressure-particle velocity Hugoniots for low-carbon steel and Composition C4, one can see that the pressure generated in the steel by the C4 is 45.9 GPa.

$$P_{C4} = (2.412\ P_{CJ}) - \left(\frac{1.7315\ P_{CJ}}{u_{CJ}}\right)u + \left(\frac{0.3195\ P_{CJ}}{u^2{}_{CJ}}\right)u^2$$

$$u_{CJ} = \frac{P_{CJ}}{\rho_0 V_D}$$

$$P_{A53} = \rho_0 C_0(u - u_0) + \rho_0 s(u - u_0)^2$$

$$P_{C4} = P_{A53}$$

$$u = 1.05\ \text{km/s}$$

$$P = 45.9\ \text{GPa}$$

Then, using the Gurney equation (25), it can be calculated that a typical steel fragment from a C4 filled pipe would have a velocity of 3.04 km/s.

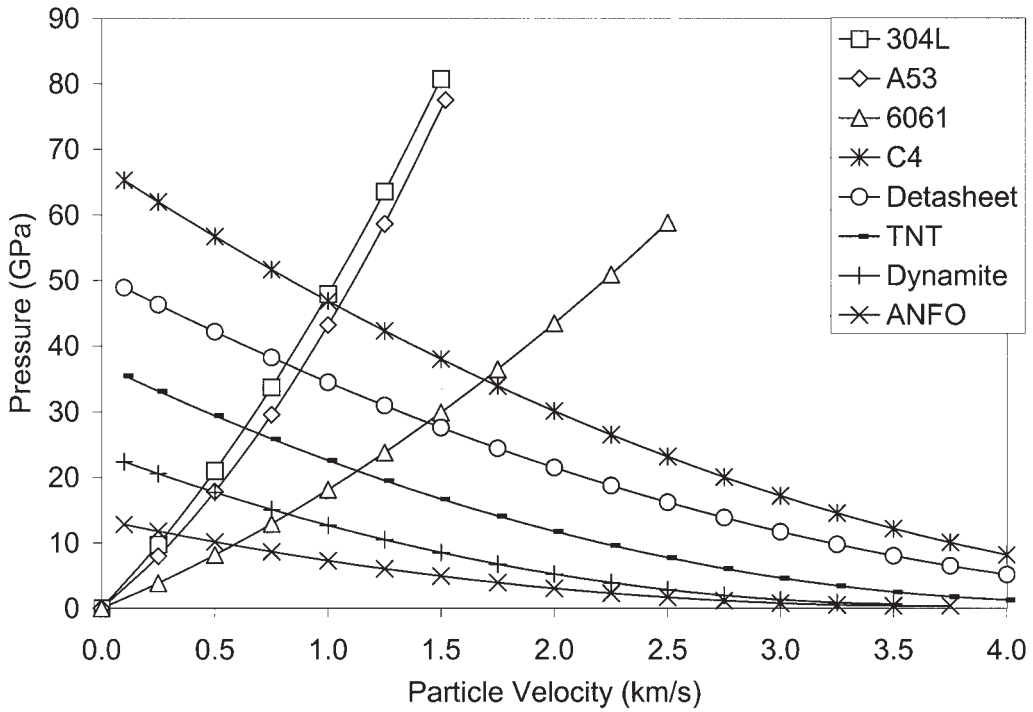

FIG. 3—*The pressure-particle velocity Hugoniots for all the explosives and metals studied. This plot can be used to graphically determine the pressure generated in a metal caused by an explosive detonation.*

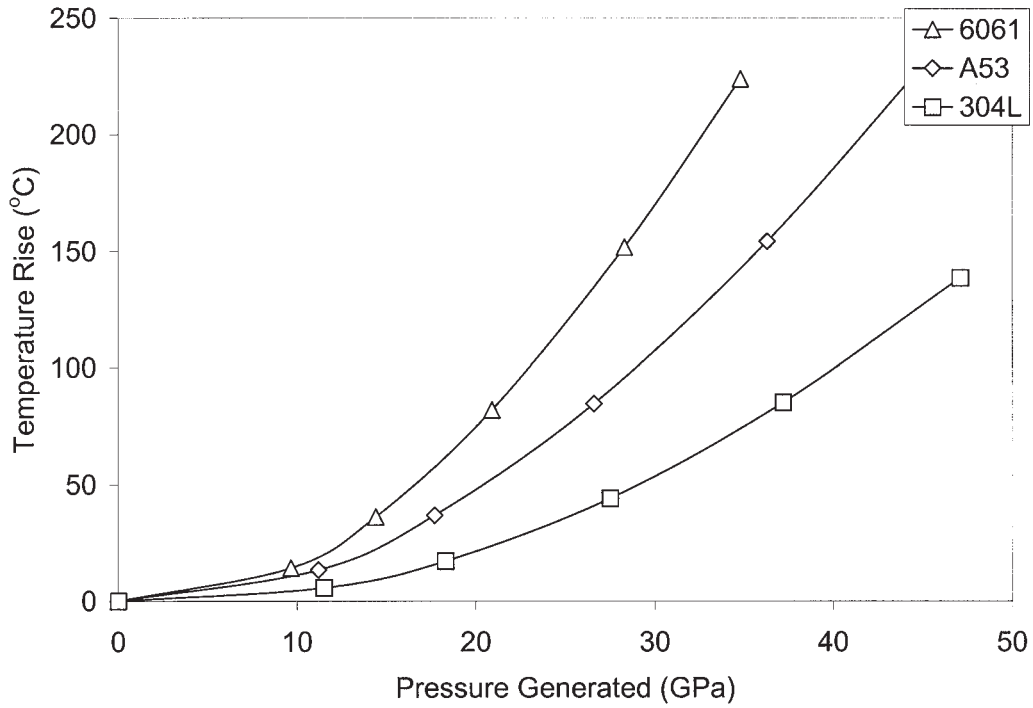

FIG. 4—*The amount of shock heating induced in each alloy by the compression of that alloy from the passage of a shock wave.*

$$\frac{V}{\sqrt{2E}} = \left(\frac{M}{C} + \frac{1}{2}\right)^{-1/2} \quad \text{where}$$

$\sqrt{2E} = 2.73 \frac{\text{km}}{\text{s}}$ is the gurney velocity of C4,

$M = 101$ g is the mass of the pipe,

$C = 327$ g is the mass of the C4, and

$V = 3.04 \frac{\text{km}}{\text{s}}$ is the velocity of a fragment.

By again equating the Hugoniots, but in this case for a steel/steel interaction with an initial velocity of 3.04 km/s, it is calculated that the pressure jumps to 77.5 GPa, which is significantly higher than the 45.9 GPa generated in steel by the detonation of C4.

$$P_{Frag} = \rho_o C_o(u - u_o) + \rho_o s(u - u_o)^2$$

$$P_{Wall} = \rho_o C_o(u - 0) + \rho_o s(u - 0)^2$$

$$P_{Frag} = P_{Wall}$$

$$u = 1.52 \text{ km/s}$$

$$P_{Frag} = 77.5 \text{ GPa}$$

These calculations indicate that interactions between any sort of metallic objects added to the pipe as shrapnel would alter the pressures seen by the metals and both the post-blast hardness and microstructure.

Microstructure

The microstructure of the fragments for all the metals tested varied so widely within each sample that it would be difficult to find a quantitative correlation between some property of the post-blast microstructure, such as grain size, and some property of the explosive used, such as detonation velocity. It is possible, however, to make qualitative comparisons of the post-blast microstructure to explosive properties. Selected fragment microstructures of A53, 304, and 6061 with regard to the detonation velocity and pressure of the explosives used are compared in Figs. 5, 6, and 7. From these figures it can be seen that, in general, the amount of deformation seen in the microstructure increases with increasing detonation velocity and pressure. This correlation between detonation velocity and the damage done to the microstructure was seen in each of the metals used in this research.

The amount of material flow seen is influenced by several initial metallurgical properties, the stacking fault energy being the main contributor to material flow under the conditions of dynamic loading (23). The stacking fault energy of a material is the energy required to create a discontinuity in the stacking arrangement of the atoms and dictates the ease of motion of dislocations through the metal matrix. When a stacking fault occurs, it is characterized by two partial dislocations, one at each end of the fault. This is also called an extended dislocation. Partial dislocations must move in tandem, which is quite difficult as it takes a great deal of energy to move a stacking fault through a material (27).

As the stacking fault energy increases, so too does the ease of dislocation motion as it is difficult to create these extended dislocations. Therefore, materials with high stacking fault energies, such as aluminum, exhibit large amounts of flow as the pressure generated by the shock wave moves these dislocations easily through the material (27).

There was little evidence of deformation twinning, though this phenomenon was prevalent in the literature (6,14). The absence of significant deformation twinning may most likely be attributed to differences in experimental setup. Experiments in which significant deformation twinning is seen are standoff operations in which a flyer plate strikes a base plate of a pure material that is sur-

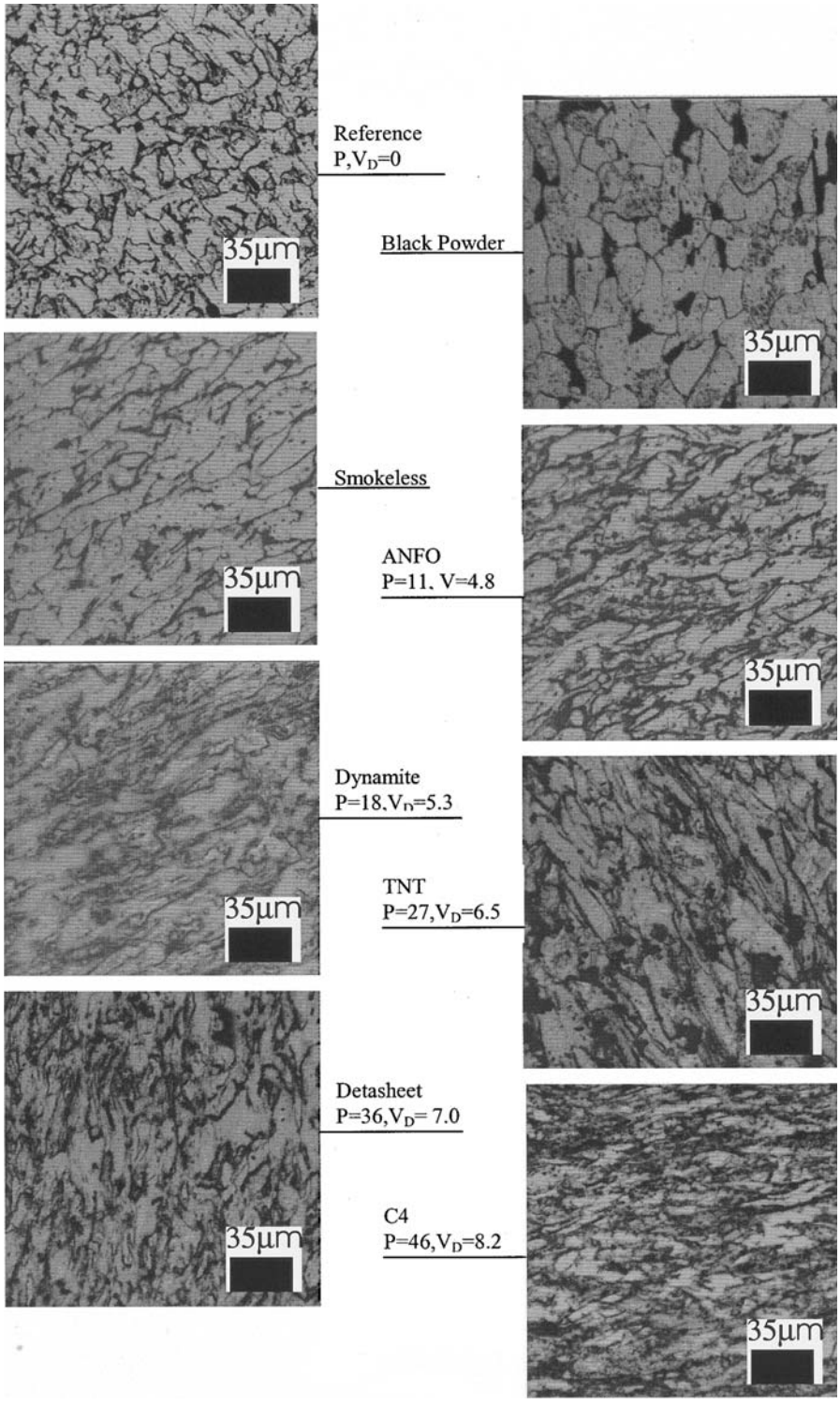

FIG. 5—*Microstructural response of A53 galvanized steel to shocks of various strengths. Both the detonation velocity of the explosive and the pressure generated increase from the top of the figure to the bottom.*

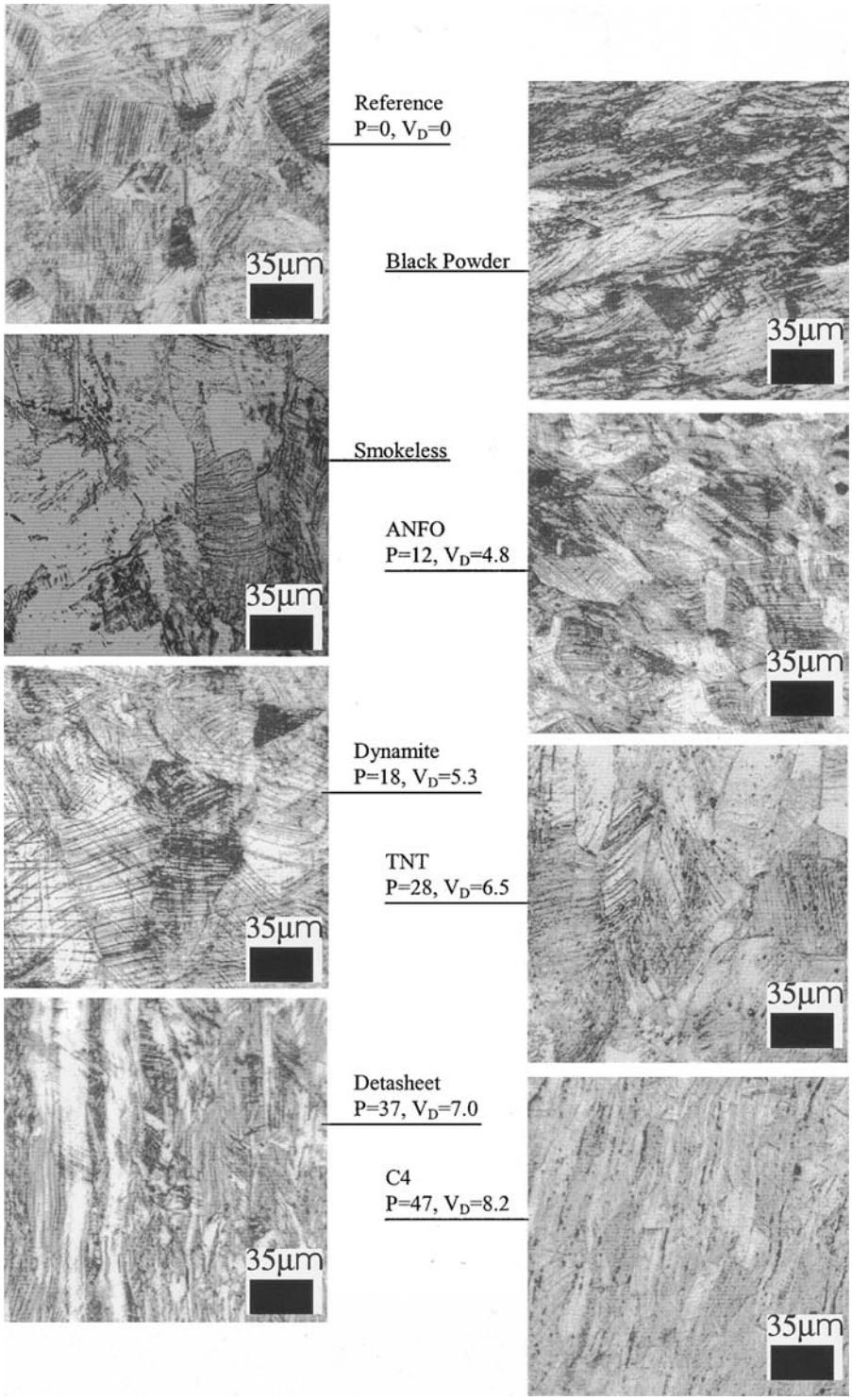

FIG. 6—*Microstructural response of 304L stainless steel to shocks of various strengths. Both the detonation velocity of the explosive and the pressure generated increase from the top of the figure to the bottom.*

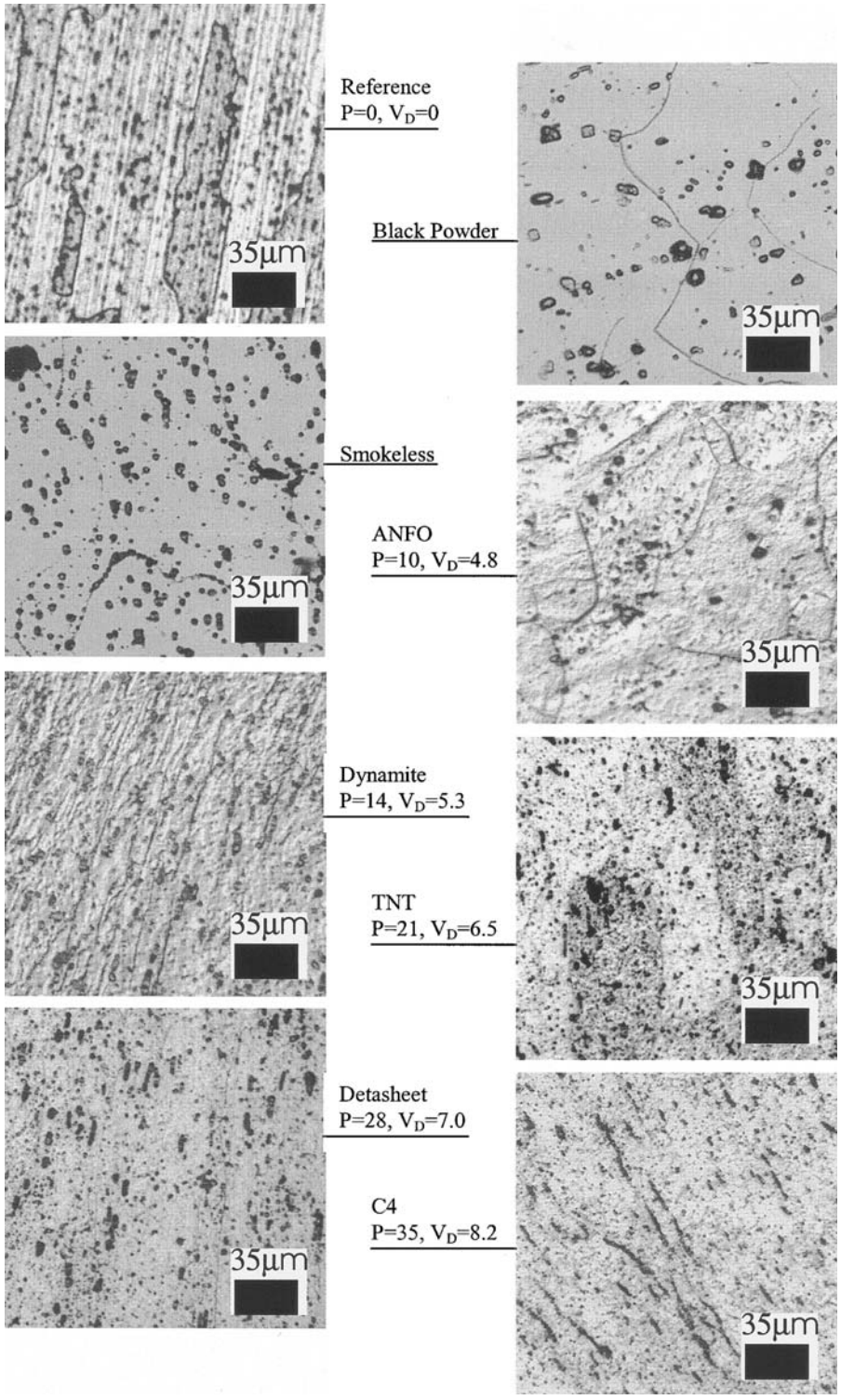

FIG. 7—*Microstructural response of 6061-T6 aluminum to shocks of various strengths. Both the detonation velocity of the explosive and the pressure generated increase from the top of the figure to the bottom.*

rounded by momentum traps. This setup generates longer pulse durations and larger pressures, which are directed along a preferred orientation.

While the microstructures and flow patterns of these post-shock fragments are interesting, and the mechanisms by which they deform should be studied to further this line of forensic investigation, it is doubtful that visual means of inspection will be able to determine the explosive used in a bombing with the degree of certainty needed in criminal investigations.

Hardness Measurements

These are the most promising methods of evaluating the shocked fragments. Not only is there a statistically significant difference in the mean pre- and post-blast fragment microhardnesses, there is a statistically significant difference found in most of the microhardness of fragments from explosive to explosive. The microhardnesses are more easily differentiable than the average macrohardness, as it was possible to perform many more Knoop tests (generally 350 and 600) than Rockwell tests (5 to 6), per sample.

The standard deviations presented for all the mean hardness values are, in most cases, greater than the error associated with the Knoop and Rockwell testers. The microhardness tests have an associated error of 2%, and the Rockwell tests have a standard error of ± 1.5. The fact that the standard deviations are larger than the error associated with testing indicates that the differences in hardness of the material are real.

The relative responses of the hardness of each metal studied to the pressures generated by the detonating explosives are shown in Figs. 8, 9 and 10. These plots show that there is a jump in hardness when there is little pressure generated in the material, then a plateau over the large, medium-pressure range, followed by a decrease towards the higher pressures in the case of aluminum. The relative change of mean hardness with detonation velocity is shown in Figs. 11,12, and 13 for each of the metals in this work. The response to detonation velocity is much the same as the response to generated pressure; there is an immediate jump, a plateau, and an annealing effect in aluminum at high-detonation velocities. The relative effect of shock heating on the hardness of the samples in this work is shown in Figs. 14, 15, and 16. These plots show the same response of hardness to shock heating as was seen for shock pressure and detonation velocity.

The response of hardness to shock loading is immediate. The mean hardness increases drastically when shocked with low velocity and pressure explosives for all the metals studied. The work hardening of the steel samples essentially plateaus in the mid- and high-range detonation velocities and pressures. The hardness of the aluminum fragments shows the same initial increase and plateau, but towards the upper end of the detonation velocities, the mean hardness falls below its initial value. The aluminum sample actually follows the same trend as the steel samples; it just experiences the plateau and the downward trend, caused by recovery and recrystallization at lower velocities and pressures than the steel samples.

As the detonation velocity of the explosive increases, so too does the strain rate of the metal. Aluminum has the highest stacking fault energy of the metals tested, and therefore the lowest number of extended dislocations, leading to the highest ease of dislocation motion, as these dislocations are not inhibited in their glide and climb. Because of this, the material can flow more readily than a metal with a low stacking fault energy. This is true for quasi-static as well as dynamic strain rates, although the effect is more pronounced at higher strain rates as the material is trying to flow very quickly so any obstacle to dislocation motion will quickly result in dislocation pile-ups and entanglements, stopping material flow. In materials with higher stacking fault energies, these dislocation pile-ups and entanglements are less likely to occur (22). Hardness is a relative measure of a material's ability to

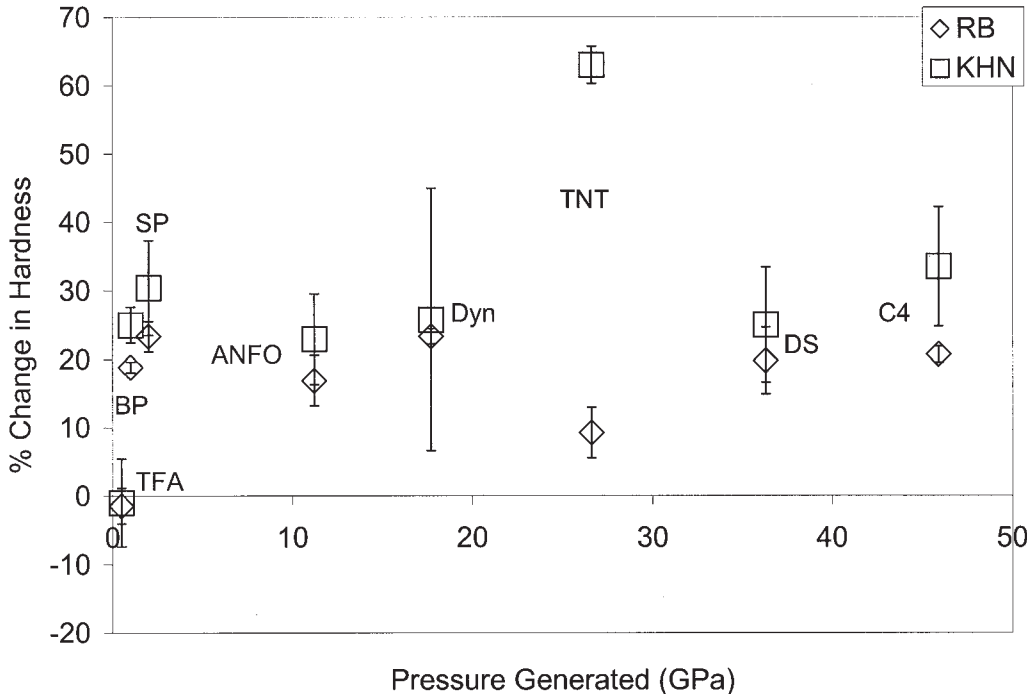

FIG. 8—*The percent change in Rockwell B (RB) and Knoop (KHN) hardness for ASTM A53 galvanized steel as a function of the pressure generated from an explosive shock.*

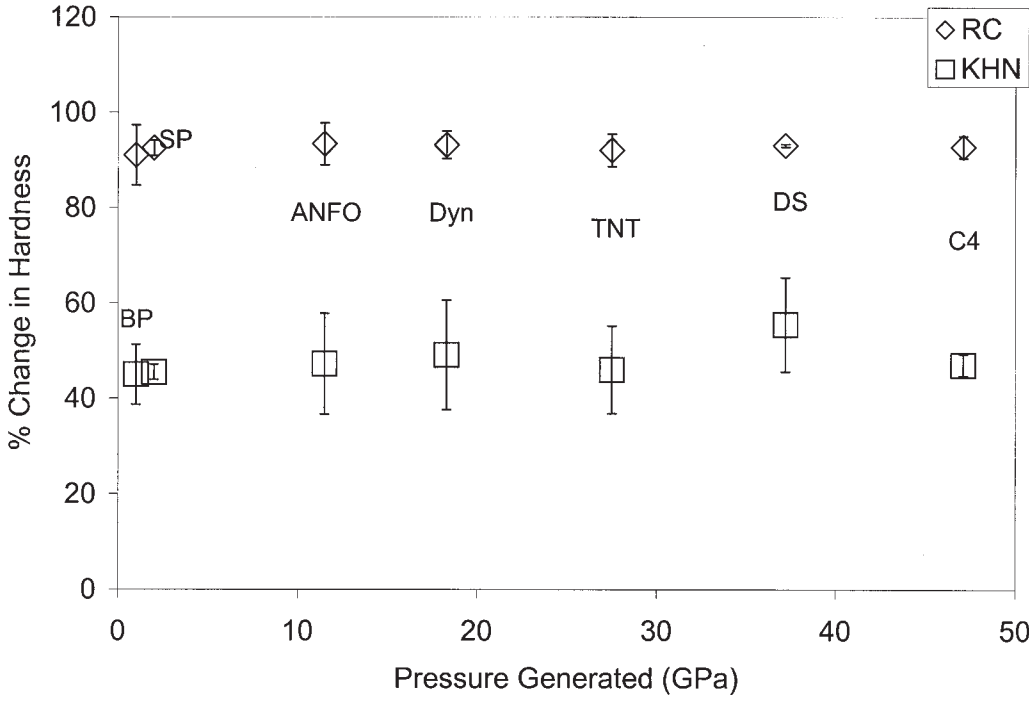

FIG. 9—*The percent change in Rockwell C (RC) and Knoop (KHN) hardness for 304L stainless steel as a function of the pressure generated from an explosive shock.*

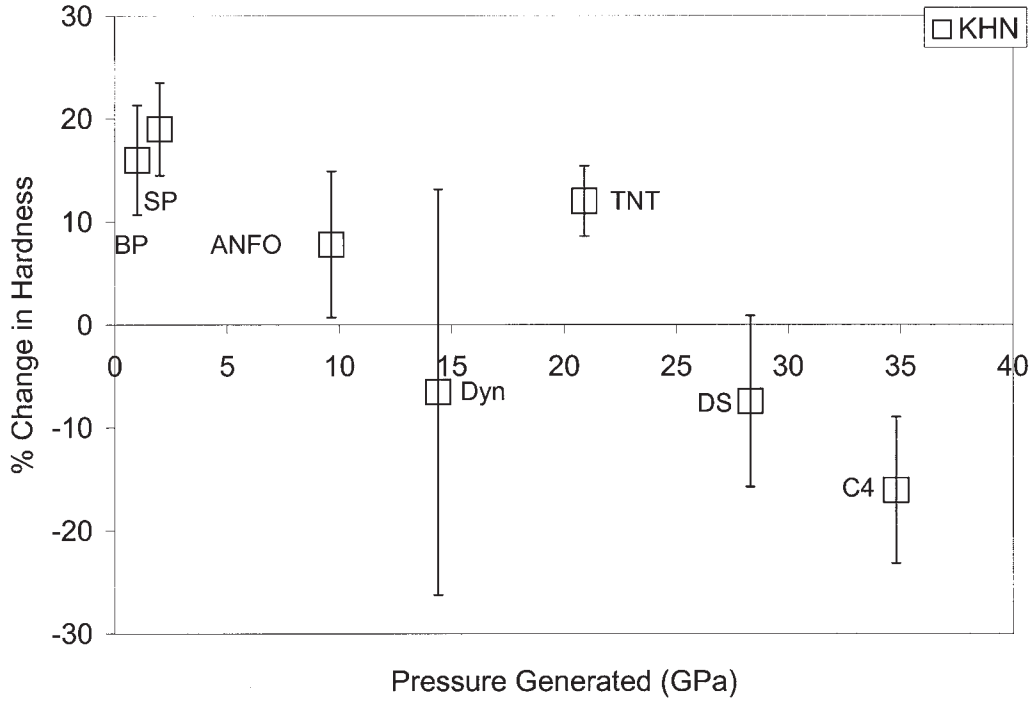

FIG. 10—*The percent change in Knoop hardness for 6061-T6 aluminum as a function of the pressure generated from an explosive shock.*

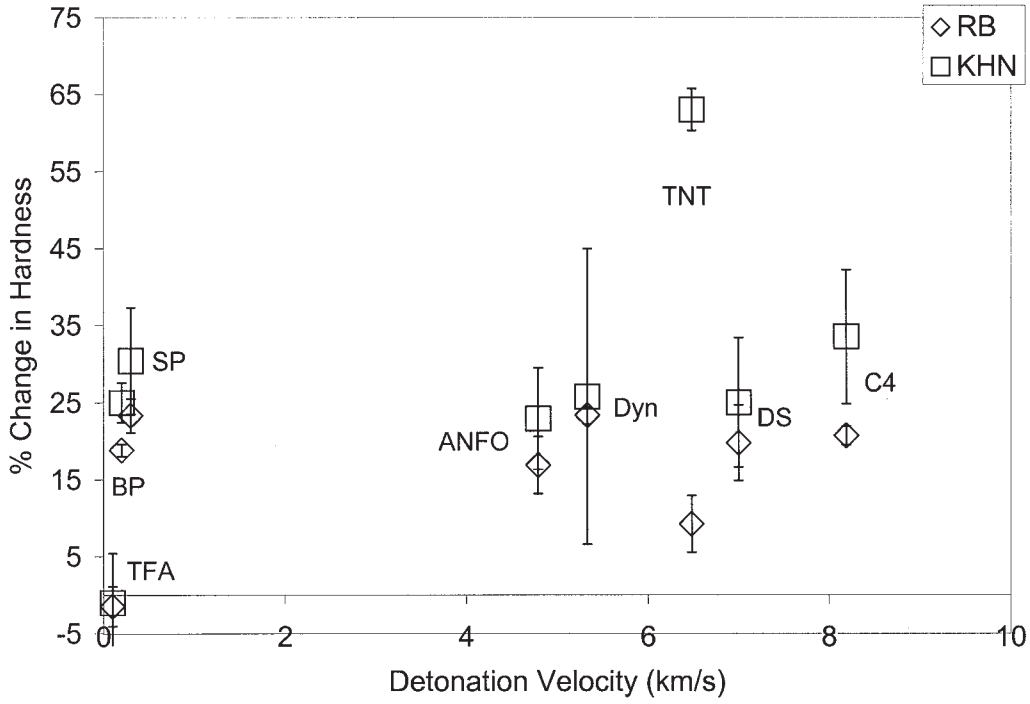

FIG. 11—*The percent change in Rockwell B (RB) and Knoop (KHN) hardness for ASTM A53 galvanized steel as a function of explosive detonation velocity.*

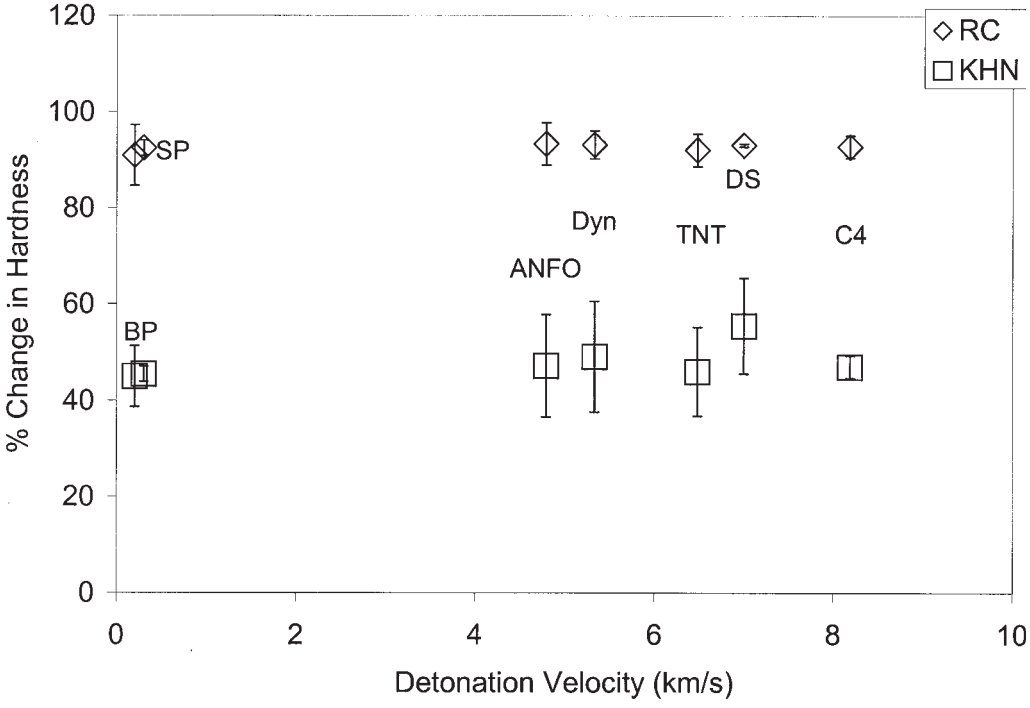

FIG. 12—*The percent change in Rockwell C (RC) and Knoop (KHN) hardness for 304L stainless steel as a function of explosive detonation velocity.*

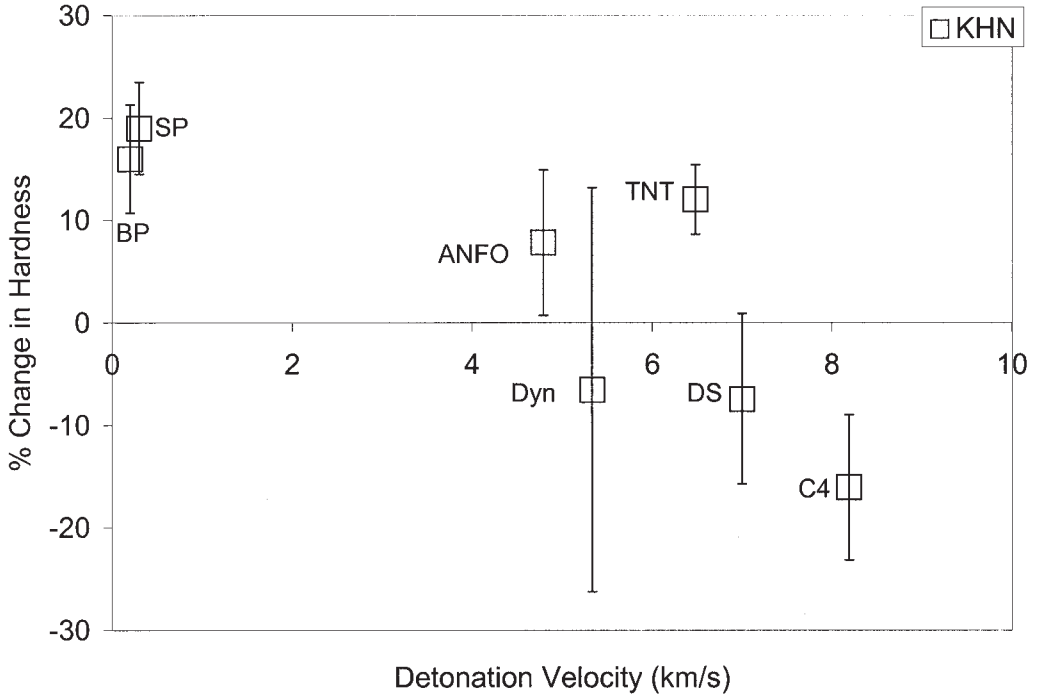

FIG. 13—*The percent change in Knoop hardness for 6061-T6 aluminum as a function of explosive detonation velocity.*

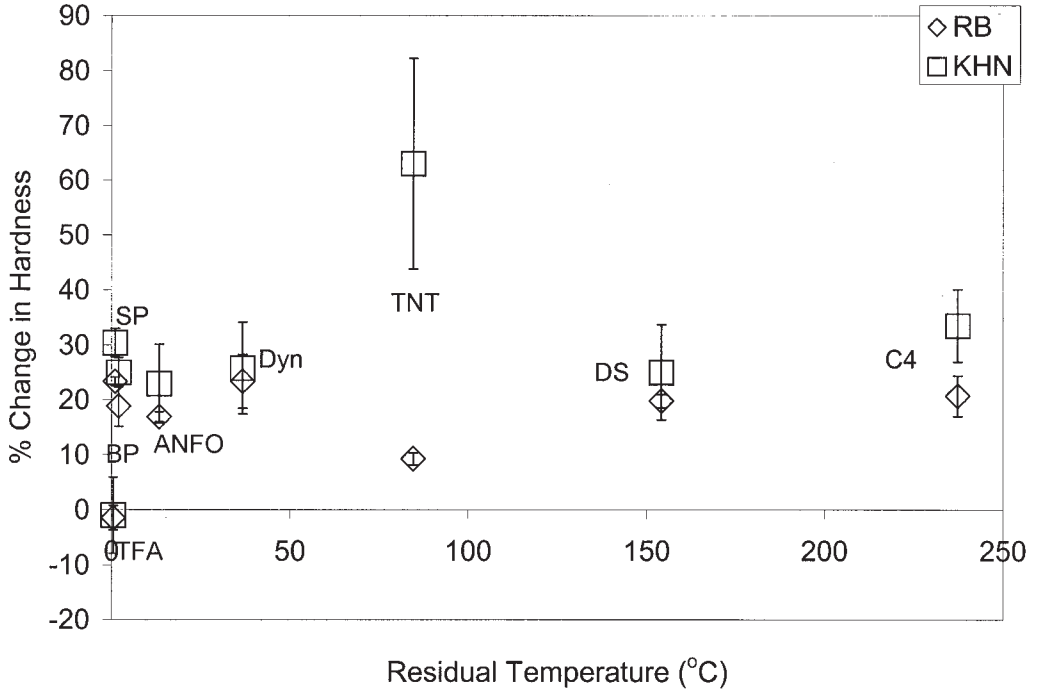

FIG. 14—*The percent change in Rockwell B (RB) and Knoop (KHN) hardness for ASTM A53 galvanized steel as a function of shock heating.*

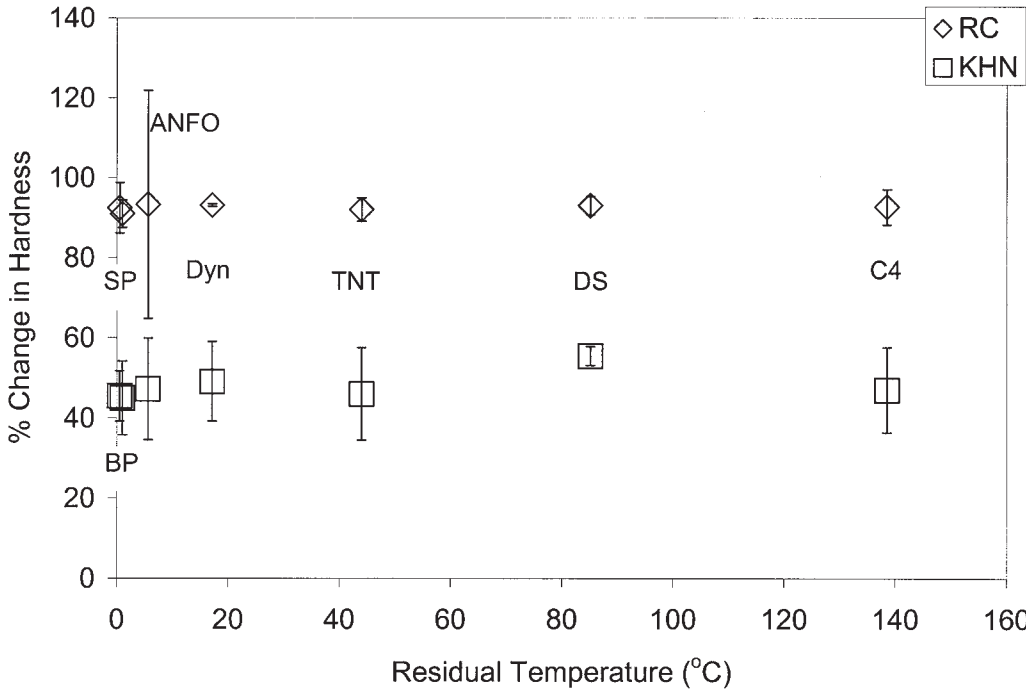

FIG. 15—*The percent change in Rockwell C (RC) and Knoop (KHN) hardness for 304L stainless steel as a function of shock heating.*

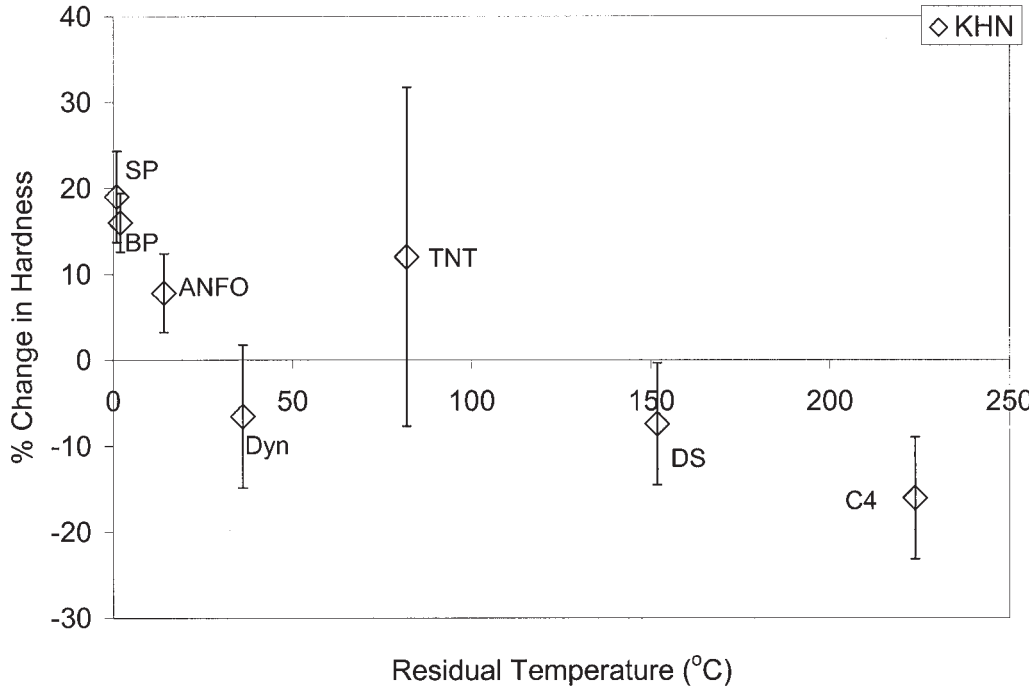

FIG. 16—*The percent change in Knoop hardness for 6061-T6 aluminum as a function of shock heating.*

flow, which is one reason why the aluminum samples shock harden to a lesser degree than the steel samples. Also, the heat generated is higher relative to the melting point for the aluminum samples than for the steels. Additionally, aluminum is subject to softening by overaging with time and temperature, whereas the steel alloys are not precipitation hardened; thus they will not soften through this mechanism.

The decrease in hardness towards the upper limits of the detonation velocities and pressures for aluminum is brought about by the shock heating generated by the explosive in each sample. As the detonation velocity increases, so too does the pressure gener-

ated in any given sample. As the pressure in the sample increases, the sample is compressed, which causes shock heating. The higher the pressure, the more heat introduced into the sample. If enough heat is put into the system, the material will begin to recover, which is a process of stress relief during which the material softens by the realignment and elimination of dislocations. The heat generated when a shock passes through a metal can be quite significant, as in the case of aluminum and steel, which are heated by over 200°C when shocked by Composition C4. This amount of heat is small compared to that released by a detonation; however, it is heat generated inside the metal rather than heat applied to the metal surface. The heat generated within the metal is conducted away more slowly and acts throughout the bulk of the metal. This time and bulk heating are required for metallurgical phenomena to occur within the metal. The melting point of aluminum is only 660°C, so the residual temperature seen by the sample is over the recrystallization temperature of 220°C (28). Also, since recrystallization was observed in small amounts in A53 fragments, as seen in Fig. 17, there must have been a tremendous amount of post-mortem heating in limited locations, as the recrystallization temperature of steel is over 625°C (28).

Fragments from the ANFO and TNT series of tests consistently show lower mean hardnesses than the other fragments in the plateau region. This may be attributed to the fact that ANFO and TNT are in prill and flake form, respectively, which leads to slight gaps between the explosive and the metal wall. This poor coupling leads to less efficient energy transfer upon detonation, which could be the cause of their relatively lower hardness values. Following this logic, it would be expected that regions of metal not in contact with the explosive (such as in incomplete filling of the pipe) would have a lower hardness than those regions that are in contact with the explosive.

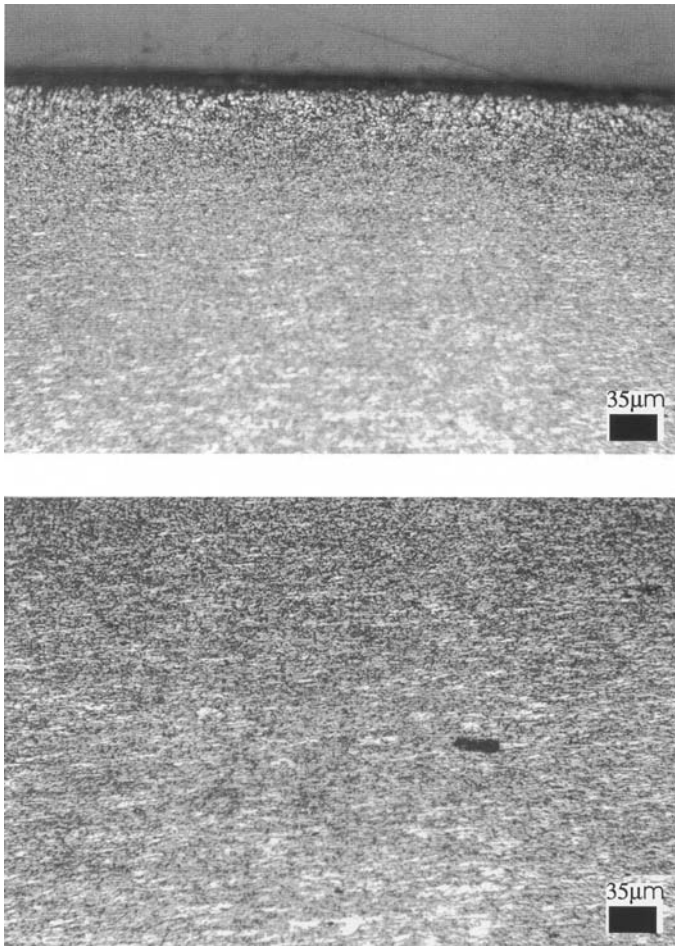

FIG. 17—*Local recrystallization seen in an A53 fragment after the detonation of Composition C4.*

TABLE 6—*The pairs of test fragments that did not show a statistically significant difference in their mean microhardness using Duncan's multiple range test.*

A53 Galvanized Steel	304L Stainless Steel	6061-T6 Aluminum
Smokeless/TNT	Detasheet/Smokeless	Smokeless/Black Powder
Detasheet/Dynamite	Detasheet/C4	Black Powder/TNT
Detasheet/ANFO	C4/Smokeless	TNT/ANFO
Jet A/Reference	Dynamite/ANFO	Detasheet/Dynamite
	Dynamite/Black Powder	
	Black Powder/ANFO	
	Black Powder/TNT	
	TNT/ANFO	

While the post-shock hardness values were similar for many of the samples, there was a statistically significant difference found between many of the microhardness means. Duncan's multiple range test was used to determine statistical significance at the 95% level (30); most of the means could be differentiated at this level of confidence; the pairs which could not be considered statistically different are listed in Table 6.

X-Ray Diffraction

The use of X-ray diffraction could be valuable in events where austenitic stainless steel pipes are used as a component in an explosive device. There was a significant increase in the presence of α' martensite in the post-blast microstructure with increasing detonation velocity and pressure; these relations can be seen in Figs. 18 and 19, respectively. The amount of martensite found in the shocked samples is quite similar to the response of hardness to shock. There is a large jump in martensite present between the shocked and reference sample, and then the amount seems to level off. The phase transformation in 304L is a process controlled by the pressure generated in the material, which is related to the detonation velocity. The increase of post-blast martensite with both pressure and detonation velocity is, therefore, expected. It is not expected, however, for this trend to continue indefinitely, as the residual temperature caused by the passage of the shock inhibits the formation of martensite. This would lead to the supposition that, at some point, the shock heating in the sample would be large enough to counter the formation of martensite.

It is important to note that the amounts of post-shocked martensite in Figs. 18 and 19 have been normalized, assuming the initial microstructure of 304L stainless steel to have no martensite present. This normalization is required, as there is error introduced by the preferred orientation of the (111) planes. This alignment is most likely brought about when the metal is rolled into sheet form before being formed into pipes. Combining and averaging the intensities of many peaks and then applying the internal standard method (25) can reduce, but never eliminate, this error. Although the error involved in these calculations essentially renders this technique qualitative in this study, the trend shown is true. There is an increase in volume percent martensite with the increase in both

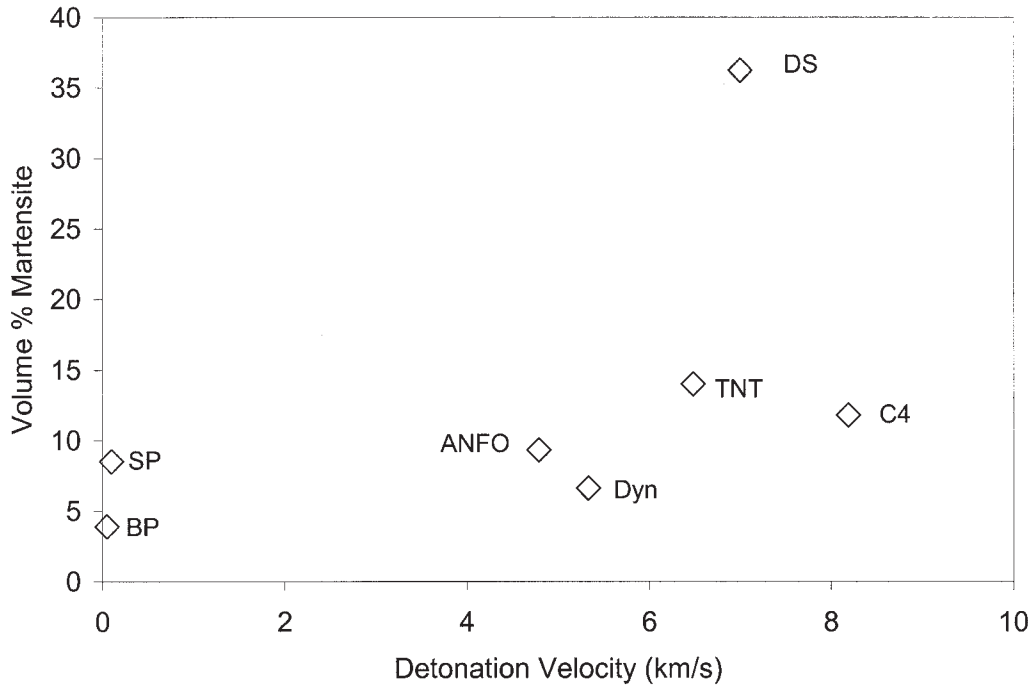

FIG. 18—*Volume percent martensite in the 304L stainless steel microstructure as a function of detonation velocity.*

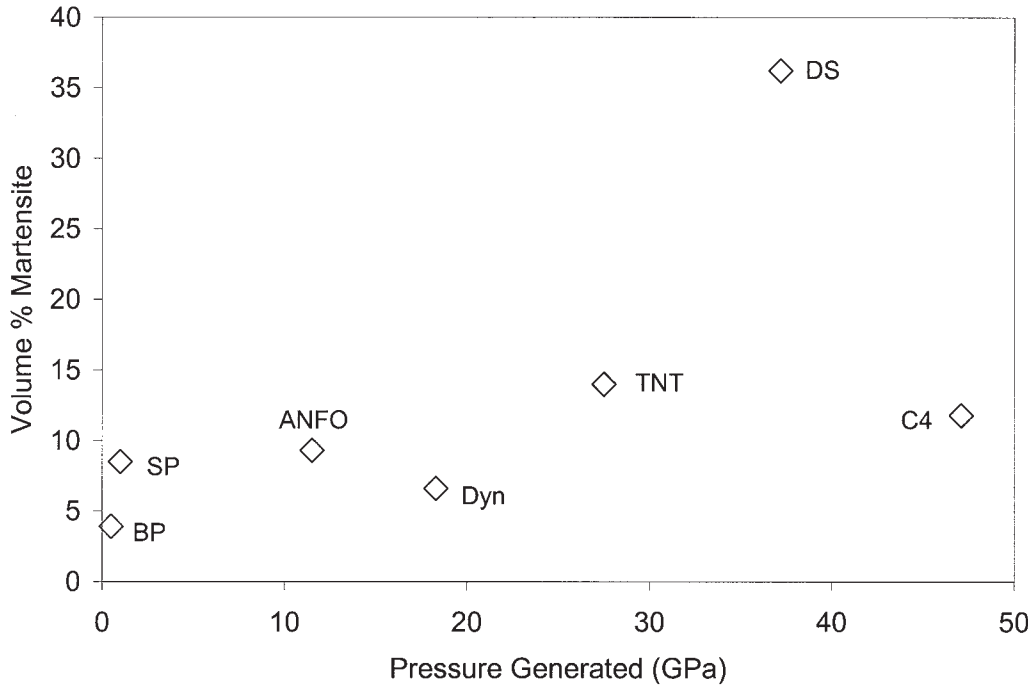

FIG. 19—*Volume percent martensite in the 304L stainless steel microstructure as a function of pressure generated by a shock.*

detonation velocity and pressure, and it is immediate. The exact degree of transformation, though, is not known.

The detasheet test showed a tremendous amount of post-blast martensite. This may be due to a manufacturing defect, such as a poor anneal after forming, or forming which did not result in recrystallization in the initial microstructure. If this pipe were poorly formed, the result would be more preferred orientation in the initial microstructure, which would further distort the results of the quantitative analysis.

Conclusions

The following trends were observed:

- Material microstructures showed increasing amounts of defor-

mation to the point of localized recrystallization in the aluminum and galvanized steel as the detonation velocity and generated pressure increased.
- The hardness of the materials studied increased immediately at low detonation velocities and pressures, exhibited a plateau over the medium detonation velocity and pressure range, and, in the case of aluminum, was shown to decrease as more powerful explosive fills were used.
- The amount of shock-induced martensite seen in 304L showed a similar response to shock as did the hardness. The amount of martensite increased at low detonation velocities and pressures, then appeared to level out as the detonation velocity and pressure continued to increase.

While this technique is essentially qualitative, with further study these methods could be used to give a range of detonation velocities and pressures of an explosive fill used in a pipe bomb, which could be very useful as a screening process for chemical examinations.

Acknowledgments

The authors would like to gratefully acknowledge the contributions of Kirk Yeager, Ph.D., from the FBI explosives lab for his valuable insight and knowledgeable contributions to this paper.

The U.S. Department of Justice Office programs must also be thanked for their generous support of this project through contract number 98-TG-CX-0001.

References

1. Oxley JC, Smith JL, Resende E, Rogers E., Strobel RA, Bender EC. Improvised explosive devices: pipe bombs. J Forensic Sci 2001;46(3): 510–34.
2. Beveridge AD. Development in the detection and identification of explosive residues. Forensic Sci Rev 1992;4(1):17–49.
3. Dahl L. Determination of black and smokeless powder residues in firearms and improvised explosive devices. Microchem J 1987;45: 40–50.
4. Garner DD, Fultz ML, Byall EB. The ATF approach to post-blast explosives detection and identification. J Energetic Mater 1986;4:133–48.
5. Kaplan, Zitrin. Identification of post-explosion residues. Journal of the AOAC 1977;60(4):619–24.
6. Crossland B. Explosive welding of metals and its application. Oxford: Clarendon Press, 1982.
7. Meyers MA. Dynamic behavior of materials. New York, NY: John Wiley & Sons Inc., 1994.
8. Zimmerly CA. Explosive welding and characterization of the bi-metallic low-carbon steel/NiTi tandem [thesis]. Socorro, NM: New Mexico Institute of Mining and Technology, 1993.
9. Kazmi B. Effects of repeated shock loading at various pressures and pulse durations during high-rate shock deformation of nickel and stainless steel 304 [thesis]. Socorro, NM: New Mexico Institute of Mining and Technology, 1979.
10. Mur, LE. Effects of peak pressure, pulse duration, and repeated loading on the residual structure and properties of shock deformed metals and alloys. In: Meyers MA, Murr, LE, editors. Shock waves and high-strain-rate phenomena in metals: concepts and applications. New York, NY: Plenum Press, 1981;753–77.
11. Staudhammer KP, Frantz CE, Hecker SS. Effects of strain rate on deformation-induced martensite in 304 stainless steel. In: Meyers MA, Murr LE, editors. Shock waves and high-strain-rate phenomena in metals: concepts and applications. New York, NY: Plenum Press, 1981;91–112.
12. Andrade U, Meyers MA, Vecchio KS, Chokski AH. Dynamic recrystallization in high-strain rate plastic deformation of copper. Acta Metallurgica et Materiala 1994;42(9):3183–95.
13. Feng C, Murr LE, Niou CS. Aspects of dynamic recrystallization in shaped charge and explosively formed projectile devices. Metallurgical and Materials Transactions A 1996;27A:1773–8.
14. Pappu S, Murr LE. Shock deformation twinning in an iron explosively formed projectile. Materials Science and Engineering A 2000;A284: 148–57.
15. Raftenberg MN, Krause CD. Metallographic observations of armor steel specimens from plates perforated by shaped charge jets. International Journal of Impact Engineering 1999;23:757–70.
16. Wittman CL. Microstructural characterization of adiabatic shear bands in low and medium carbon steels [thesis]. Socorro, NM: New Mexico Institute of Mining and Technology, 1985.
17. Shockey DA, Elrich DC. Metallurgical influences on shear band activity. In: Meyers MA, Murr LE, editors. Shock waves and high-strain-rate phenomena in metals: concepts and applications. New York, NY: Plenum Press, 1981;249–61.
18. Barbieri F, Montanari R. X-ray study on shock loaded AISI 304 steel. Materials Letters 1991;10(9,10):453–6.
19. Dickson MJ. The significance of texture parameters in phase analysis by X-ray diffraction. Journal of Applied Chrystallography 1969;2:176–80.
20. Moin E, Murr LE. Interactive effects of shock loading parameters on the substructure and mechanical properties of nickel and stainless steel. Materials Science and Engineering 1979;37:249–69.
21. Staudhammer KP. Effect of shock stress amplitude, shock stress duration, and prior deformation on the residual microstructure of explosively deformed stainless steels [dissertation]. Socorro, NM: New Mexico Institute of Mining and Technology, 1975.
22. Murr LE, Inal OT, Morales AA. Direct observation of vacancies and vacancy-type defects in molybdenum following uniaxial shock wave compression. Acta Metallurgica 1976;24:264–70.
23. Murr LE, Inal OT, Morales AA. Vacancies and vacancy clusters in shock-loaded molybdenum: direct observations by transmission electron and field-ion microscopy. Applied Physics Letters 1976;28(8):432–4.
24. Petzow G. Metallographic etching. 2nd ed. Materials Park, OH: ASM International, 1999;57–64,94–102.
25. Cullity BD. Elements of X-ray diffraction. 2nd ed. Reading, MA: Addison Wesley Publishing Company, Inc., 1978;411–15, 508–22.
26. Cooper PW. Explosives engineering. New York, NY: John Wiley & Sons Inc., 1996;46–50,267–8.
27. McQueen RG, Marsh SP, Taylor JW, Fritz HN, Carter WJ. The equation of state of solids from shock wave studies. In: Kinslow, R, editor. High velocity impact phenomena. New York, NY: Academic Press, 1970; Chapter 30.
28. Reed-Hill RE, Abbaschian R. Physical metallurgy principles. 3rd ed. Boston, MA: PWS Publishing Company, 1994;102–13.
29. Kalpakjian S. Manufacturing processes for engineering materials. Menlo Park, CA: Addison Wesley Longman Inc, 1997;104.
30. Montgomery DC. Design and analysis of experiments. New York, NY: John Wiley & Sons Inc, 1997;103–5,675.

Additional information and reprint requests:
Graham Walsh
Department of Materials and Metallurgical Engineering
801 Leroy Place
Socorro, NM 87801